Signal Processing Seminars

On the use of Gabor Filters in SOS Corrected Ultrasound Image Segmentation

Augustin Cosse, Damien Bouvy

Université Catholique de Louvain – Ecole Polytechnique de Louvain

ICTEAM Institute

December 2011

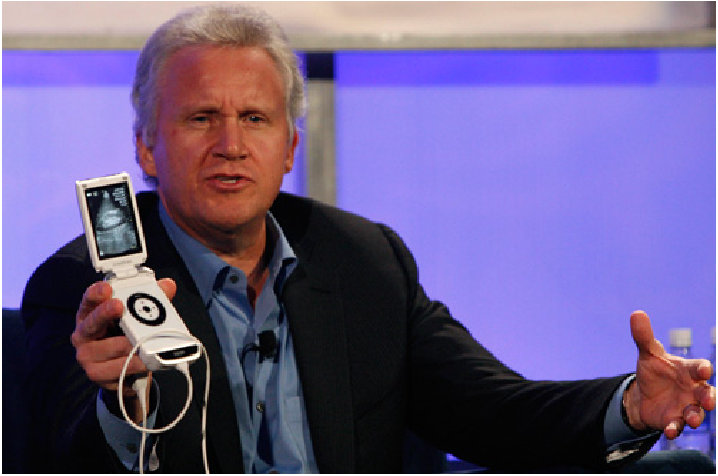

Small is big : Jeff Immelt is seen here unveiling the new Vscan technology (i.e portable Ultrasound) to the audience at Web 2.0 Summit in San Francisco (see http ://www.gereports.com).

However, a recent study on mice from Yale University [Ang 06] showed that exposure to ultrasound while pregnant may affect brain development in the fetus.

Too soon to extrapolate the findings to humans.

It may be that the ultrasound waves somehow disrupt the connections formed between cells as they move into their proper location

As a conclusion, beautifull modality...Whose effects still need to be studied

However, a recent study on mice from Yale University [Ang 06] showed that exposure to ultrasound while pregnant may affect brain development in the fetus.

Too soon to extrapolate the findings to humans.

It may be that the ultrasound waves somehow disrupt the connections formed between cells as they move into their proper location

As a conclusion, beautifull modality...Whose effects still need to be studied

However, a recent study on mice from Yale University [Ang 06] showed that exposure to ultrasound while pregnant may affect brain development in the fetus.

Too soon to extrapolate the findings to humans.

It may be that the ultrasound waves somehow disrupt the connections formed between cells as they move into their proper location

As a conclusion, beautifull modality...Whose effects still need to be studied

However, a recent study on mice from Yale University [Ang 06] showed that exposure to ultrasound while pregnant may affect brain development in the fetus.

Too soon to extrapolate the findings to humans.

It may be that the ultrasound waves somehow disrupt the connections formed between cells as they move into their proper location

As a conclusion, beautifull modality...Whose effects still need to be studied

However, a recent study on mice from Yale University [Ang 06] showed that exposure to ultrasound while pregnant may affect brain development in the fetus.

Too soon to extrapolate the findings to humans.

It may be that the ultrasound waves somehow disrupt the connections formed between cells as they move into their proper location

As a conclusion, beautifull modality...Whose effects still need to be studied

The basic principle of ultrasound imaging is simple.

A propagating wave partially reflects at the interface between tissues.

If these reflections are measured as a function of time, information is obtained on the position of the tissue

The basic principle of ultrasound imaging is simple.

A propagating wave partially reflects at the interface between tissues.

If these reflections are measured as a function of time, information is obtained on the position of the tissue

The basic principle of ultrasound imaging is simple.

A propagating wave partially reflects at the interface between tissues.

If these reflections are measured as a function of time, information is obtained on the position of the tissue

The main instrumentation in US imaging consist of a transducer.

This tranducer acts both as a transmitter and signal receiver

The transmission mode converts an oscillating voltage into mechanical vibrations transmitted as pressure waves

Total pressure at position x is then given by
$p_T(x,t) = p_0 + p(x,t)$ [Hill 04]

The main instrumentation in US imaging consist of a transducer.

This tranducer acts both as a transmitter and signal receiver

The transmission mode converts an oscillating voltage into mechanical vibrations transmitted as pressure waves

Total pressure at position x is then given by $p_T(x,t) = p_0 + p(x,t)$ [Hill 04]

The main instrumentation in US imaging consist of a transducer.

This tranducer acts both as a transmitter and signal receiver

The transmission mode converts an oscillating voltage into mechanical vibrations transmitted as pressure waves

Total pressure at position x is then given by $p_T(x,t) = p_0 + p(x,t)$ [Hill 04]

The main instrumentation in US imaging consist of a transducer.

This tranducer acts both as a transmitter and signal receiver

The transmission mode converts an oscillating voltage into mechanical vibrations transmitted as pressure waves

Total pressure at position x is then given by
$p_T(x,t) = p_0 + p(x,t)$ [Hill 04]

Developping and simplifying, we found the following wave equation.

$$\nabla^2 p - \frac{1}{C^2}\frac{\partial^2 p}{\partial^2 t} = 0$$ [Hill 04]

Where $C \equiv \frac{1}{\sqrt{\rho_0 \beta_0}}$ is the speed of sound (SOS)

With ρ and β the values of the density and compressibility resp.

Developping and simplifying, we found the following wave equation.

$$\nabla^2 p - \frac{1}{C^2}\frac{\partial^2 p}{\partial^2 t} = 0$$ [Hill 04]

Where $C = \frac{1}{\sqrt{\rho_0 \beta_0}}$ is the speed of sound (SOS)

With ρ and β the values of the density and compressibility resp.

Developping and simplifying, we found the following wave equation.

$$\nabla^2 p - \frac{1}{C^2}\frac{\partial^2 p}{\partial^2 t} = 0$$ [Hill 04]

Where $C \equiv \frac{1}{\sqrt{\rho_0 \beta_0}}$ is the speed of sound (SOS)

With ρ and β the values of the density and compressibility resp.

Developping and simplifying, we found the following wave equation.

$$\nabla^2 p - \frac{1}{C^2}\frac{\partial^2 p}{\partial^2 t} = 0$$ [Hill 04]

Where $C \equiv \frac{1}{\sqrt{\rho_0 \beta_0}}$ is the speed of sound (SOS)

With ρ and β the values of the density and compressibility resp.

Tissue type	Density (g/cm^3)	Speed of sound (m/s)
Connective	1.120	1613
Muscle	1.050	1547
Fat	0.950	1478
Adipose	0.950	1450
Blood	1.060	1584
Brain	1.040	1560
Breast	1.020	1510
Kidney	1.050	1560
Liver	1.060	1595
Muscle, cardiac	1.060	1576
Muscle, skeletal	1.050	1580
Skin	1.090	1615
Average soft tissue: Fatty	0.985	1465
Average soft tissue: Non-fatty	1.055	1575
Blood cells	1.093	1627
Blood plasma	1.027	1543
Spinal cord	1.038	1542
Spleen	1.054	1567
Testis	1.044	1595
Mean	1.042	1557
Standard deviation	0.043	50

Current Ultrasound devices assume that SOS is constant in all tissues (1540 m/s) [Fontanarosa 11]

In soft human tissues :

$SOS = ((1.09) \cdot \rho + 0.419) \cdot 10^3 m/s \pm 3.5 m/s$

Current Ultrasound devices assume that SOS is constant in all tissues (1540 m/s) [Fontanarosa 11]

In soft human tissues :
$SOS = ((1.09) \cdot \rho + 0.419) \cdot 10^3 m/s \pm 3.5 m/s$

Using the Hounsfield units of CT scans, it is possible to define a density map of the body

Then using this density map, one can compute a SOS map using the linear relation of previous slide

Briefly, penetration depth in current devices is computed as $d = \frac{TOF}{2}\tilde{SOS}$ with $\tilde{SOS} = 1540\,m/s$ is the speed of sound (SOS)

Wherever actual penetration depth is given by $d_{corr} = \frac{1}{2}\sum_{j=1}^{n} SOS_j(TOF_j - TOF_{j-1})$

Using the Hounsfield units of CT scans, it is possible to define a density map of the body

Then using this density map, one can compute a SOS map using the linear relation of previous slide

Briefly, penetration depth in current devices is computed as $d = \frac{TOF}{2}\tilde{SOS}$ with $\tilde{SOS} = 1540\,m/s$ is the speed of sound (SOS)

Wherever actual penetration depth is given by $d_{corr} = \frac{1}{2}\sum_{j=1}^{n} SOS_j(TOF_j - TOF_{j-1})$

Using the Hounsfield units of CT scans, it is possible to define a density map of the body

Then using this density map, one can compute a SOS map using the linear relation of previous slide

Briefly, penetration depth in current devices is computed as $d = \frac{TOF}{2}\tilde{SOS}$ with $\tilde{SOS} = 1540\, m/s$ is the speed of sound (SOS)

Wherever actual penetration depth is given by $d_{corr} = \frac{1}{2}\sum_{j=1}^{n} SOS_j (TOF_j - TOF_{j-1})$

Using the Hounsfield units of CT scans, it is possible to define a density map of the body

Then using this density map, one can compute a SOS map using the linear relation of previous slide

Briefly, penetration depth in current devices is computed as $d = \frac{TOF}{2}\tilde{SOS}$ with $\tilde{SOS} = 1540\, m/s$ is the speed of sound (SOS)

Wherever actual penetration depth is given by

$$d_{corr} = \frac{1}{2}\sum_{j=1}^{n} SOS_j(TOF_j - TOF_{j-1})$$

And every voxel has to be resized in the axial direction from $d_i = \frac{1}{2}\tilde{SOS} \cdot (TOF_i - TOF_{i-1})$ to $d_{i,corr} = \frac{1}{2}SOS_i \cdot (TOF_i - TOF_{i-1})$

We then use an axial scaling factor given by $\Delta = \frac{SOS_i}{\tilde{SOS}} d_i$

And every voxel has to be resized in the axial direction from $d_i = \frac{1}{2}\tilde{SOS} \cdot (TOF_i - TOF_{i-1})$ to $d_{i,corr} = \frac{1}{2}SOS_i \cdot (TOF_i - TOF_{i-1})$

We then use an axial scaling factor given by $\Delta = \frac{SOS_i}{\tilde{SOS}} d_i$

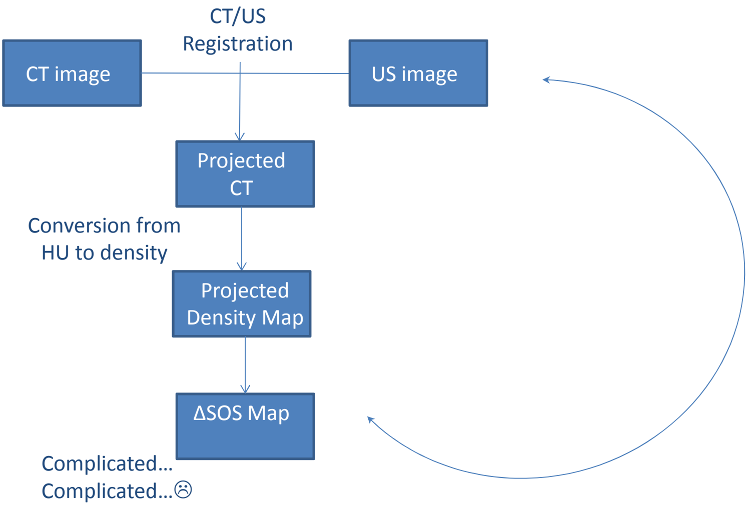
CT/US
Registration
CT image
US image
Projected
CT
Conversion from
HU to density
Projected
Density Map
ΔSOS Map
Complicated…
Complicated…☹

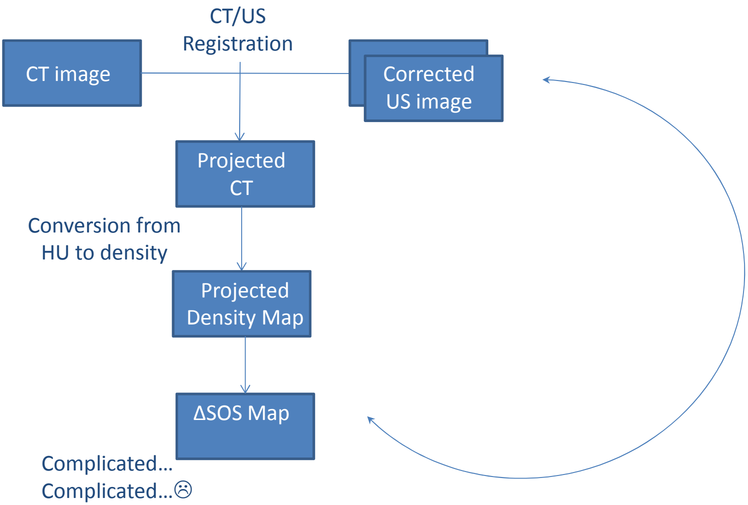
CT/US
Registration
CT image
Corrected
US image
Projected
CT
Conversion from
HU to density
Projected
Density Map
ΔSOS Map
Complicated…
Complicated…☹

Gabor Filtering and Classification

Once US Images have been corrected for SOS aberrations, We propose to consider the approach of [Zhan 06]

The approach consists of 2 steps :

- Training
- Application

Gabor Filtering and Classification

Once US Images have been corrected for SOS aberrations, We propose to consider the approach of [Zhan 06]

The approach consists of 2 steps :

- Training
- Application

Gabor Filtering and Classification

Once US Images have been corrected for SOS aberrations, We propose to consider the approach of [Zhan 06]

The approach consists of 2 steps :

- Training
- Application

Gabor Filtering and Classification

Once US Images have been corrected for SOS aberrations, We propose to consider the approach of [Zhan 06]

The approach consists of 2 steps :

- Training
- Application

Gabor Filtering and Classification

- During training, shape and tecture priors are extracted from training images
- Then an anisotropic median filtering is applied to reduce the speckle noise from the test images
- Finally Support vector machines are used to label voxels based on their texture features

Once the texture classification has been completed, the organ shape is moved at the boundary between voxels classified as organ and non-organ

Gabor Filtering and Classification

- During training, shape and tecture priors are extracted from training images
- Then an anisotropic median filtering is applied to reduce the speckle noise from the test images
- Finally Support vector machines are used to label voxels based on their texture features

Once the texture classification has been completed, the organ shape is moved at the boundary between voxels classified as organ and non-organ

Gabor Filtering and Classification

- During training, shape and tecture priors are extracted from training images

- Then an anisotropic median filtering is applied to reduce the speckle noise from the test images

- Finally Support vector machines are used to label voxels based on their texture features

Once the texture classification has been completed, the organ shape is moved at the boundary between voxels classified as organ and non-organ

Gabor Filtering and Classification

- During training, shape and tecture priors are extracted from training images
- Then an anisotropic median filtering is applied to reduce the speckle noise from the test images
- Finally Support vector machines are used to label voxels based on their texture features

Once the texture classification has been completed, the organ shape is moved at the boundary between voxels classified as organ and non-organ

Those 2 steps (texture classification + shape deformation) are repeated untill convergence

Gabor filtering and SVM Classification are performed on subsurfaces

I.e. Let us define our shape as a set of vertices $S = \{P_i,\ i = 1,\ ...,\ I\}$.

Let us note T a set of triangles where $T = \{Tr_i,\ i = 1,\ ...,\ I\}$ and $Tr_j = \left\{P_1^j, P_2^j, P_3^j\right\}$

Then the entire surface is decomposed into N subsurfaces $S_k = \left\{Tr_l^k,\ l = 1,\ ...,\ N_k\right\}$

Those 2 steps (texture classification + shape deformation) are repeated untill convergence

Gabor filtering and SVM Classification are performed on subsurfaces

I.e. Let us define our shape as a set of vertices $S = \{P_i,\ \ i = 1,\ ...,\ I\}$.

Let us note T a set of triangles where $T = \{Tr_i,\ \ i = 1,\ ...,\ I\}$ and $Tr_j = \left\{P_1^j, P_2^j, P_3^j\right\}$

Then the entire surface is decomposed into N subsurfaces $S_k = \left\{Tr_l^k,\ \ l = 1,\ ...,\ N_k\right\}$

Those 2 steps (texture classification + shape deformation) are repeated untill convergence

Gabor filtering and SVM Classification are performed on subsurfaces

I.e. Let us define our shape as a set of vertices $S = \{P_i,\ \ i = 1,\ ...,\ I\}$.

Let us note T a set of triangles where $T = \{Tr_i,\ \ i = 1,\ ...,\ I\}$ and $Tr_j = \left\{P_1^j, P_2^j, P_3^j\right\}$

Then the entire surface is decomposed into N subsurfaces $S_k = \left\{Tr_l^k,\ \ l = 1,\ ...,\ N_k\right\}$

Those 2 steps (texture classification + shape deformation) are repeated untill convergence

Gabor filtering and SVM Classification are performed on subsurfaces

I.e. Let us define our shape as a set of vertices $S = \{P_i,\ \ i = 1,\ ...,\ I\}$.

Let us note T a set of triangles where $T = \{Tr_i,\ \ i = 1,\ ...,\ I\}$ and $Tr_j = \left\{P_1^j,\, P_2^j,\, P_3^j\right\}$

Then the entire surface is decomposed into N subsurfaces $S_k = \{Tr_l^k,\ \ l = 1,\ ...,\ N_k\}$

Those 2 steps (texture classification + shape deformation) are repeated untill convergence

Gabor filtering and SVM Classification are performed on subsurfaces

I.e. Let us define our shape as a set of vertices $S = \{P_i,\ i = 1,\ ...,\ I\}$.

Let us note T a set of triangles where $T = \{Tr_i,\ i = 1,\ ...,\ I\}$ and $Tr_j = \left\{P_1^j, P_2^j, P_3^j\right\}$

Then the entire surface is decomposed into N subsurfaces $S_k = \left\{Tr_l^k,\ l = 1,\ ...,\ N_k\right\}$

To save computation time, two gabor filter banks located at 2 orthogonal planes (axial and coronal) are used

$$g_{\gamma,\omega}(x,y) = a^{\gamma} g(a^{\gamma}(x\cos(\omega\psi) + y\sin(\omega\psi)), a^{\gamma}(-x\sin(\omega\psi) + y\cos(\omega\psi))) \quad (1)$$

$$h_{\gamma,\omega}(y,z) = a^{\gamma} h(a^{\gamma}(y\cos(\omega\psi) + z\sin(\omega\psi)), a^{\gamma}(-y\sin(\omega\psi) + z\cos(\omega\psi))) \quad (2)$$

$$(\gamma = 0,\ldots,\Gamma-1 \;\; \omega = 0,\ldots,\Omega-1)$$

To save computation time, two gabor filter banks located at 2 orthogonal planes (axial and coronal) are used

$$g_{\gamma,\omega}(x,y) = a^{\gamma} g(a^{\gamma}(x\cos(\omega\psi) + y\sin(\omega\psi)), a^{\gamma}(-x\sin(\omega\psi) + y\cos(\omega\psi))) \quad (1)$$

$$h_{\gamma,\omega}(y,z) = a^{\gamma} h(a^{\gamma}(y\cos(\omega\psi) + z\sin(\omega\psi)), a^{\gamma}(-y\sin(\omega\psi) + z\cos(\omega\psi))) \quad (2)$$

$$(\gamma = 0, \ldots, \Gamma - 1 \;\; \omega = 0, \ldots, \Omega - 1)$$

Application of GF on each voxel gives 4 sets of texture features

$$\left\{\hat{G}^{real}_{\gamma,\omega}(\vec{v})\right\}, \ \left\{\hat{G}^{img}_{\gamma,\omega}(\vec{v})\right\}, \left\{\hat{H}^{real}_{\gamma,\omega}(\vec{v})\right\}, \ \left\{\hat{H}^{img}_{\gamma,\omega}(\vec{v})\right\}$$

Gabor features are then compiled into a vector $T(\vec{v})$

This vector is then used to classify the voxels as organ and non organ using KSVM

Application of GF on each voxel gives 4 sets of texture features

$$\left\{\hat{G}^{real}_{\gamma,\omega}(\vec{v})\right\}, \quad \left\{\hat{G}^{img}_{\gamma,\omega}(\vec{v})\right\}, \left\{\hat{H}^{real}_{\gamma,\omega}(\vec{v})\right\}, \quad \left\{\hat{H}^{img}_{\gamma,\omega}(\vec{v})\right\}$$

Gabor features are then compiled into a vector $T(\vec{v})$

This vector is then used to classify the voxels as organ and non organ using KSVM

Application of GF on each voxel gives 4 sets of texture features

$$\left\{\hat{G}^{real}_{\gamma,\omega}(\vec{v})\right\},\ \left\{\hat{G}^{img}_{\gamma,\omega}(\vec{v})\right\},\left\{\hat{H}^{real}_{\gamma,\omega}(\vec{v})\right\},\ \left\{\hat{H}^{img}_{\gamma,\omega}(\vec{v})\right\}$$

Gabor features are then compiled into a vector $T(\vec{v})$

This vector is then used to classify the voxels as organ and non organ using KSVM

Application of GF on each voxel gives 4 sets of texture features

$$\left\{\hat{G}^{real}_{\gamma,\omega}(\vec{v})\right\},\ \left\{\hat{G}^{img}_{\gamma,\omega}(\vec{v})\right\},\left\{\hat{H}^{real}_{\gamma,\omega}(\vec{v})\right\},\ \left\{\hat{H}^{img}_{\gamma,\omega}(\vec{v})\right\}$$

Gabor features are then compiled into a vector $T(\vec{v})$

This vector is then used to classify the voxels as organ and non organ using KSVM

Kernel Support Vector Machines

Given m samples, KSVM gives a decision plane which separates positive samples from negative ones

KSVM are first trained using the texture vectors coming from organ and non organ tissue

Then during application step, KSVM are used to classify voxels based on their texture properties $\vec{T}(\vec{v})$

KSVM gives the signed distance from $\vec{T}(\vec{v})$ to the separation hyperplane

Kernel Support Vector Machines

Given m samples, KSVM gives a decision plane which separates positive samples from negative ones

KSVM are first trained using the texture vectors coming from organ and non organ tissue

Then during application step, KSVM are used to classify voxels based on their texture properties $\vec{T}(\vec{v})$

KSVM gives the signed distance from $\vec{T}(\vec{v})$ to the separation hyperplane

Kernel Support Vector Machines

Given m samples, KSVM gives a decision plane which separates positive samples from negative ones

KSVM are first trained using the texture vectors coming from organ and non organ tissue

Then during application step, KSVM are used to classify voxels based on their texture properties $\vec{T}(\vec{v})$

KSVM gives the signed distance from $\vec{T}(\vec{v})$ to the separation hyperplane

Kernel Support Vector Machines

Given m samples, KSVM gives a decision plane which separates positive samples from negative ones

KSVM are first trained using the texture vectors coming from organ and non organ tissue

Then during application step, KSVM are used to classify voxels based on their texture properties $\vec{T}(\vec{v})$

KSVM gives the signed distance from $\vec{T}(\vec{v})$ to the separation hyperplane

Kernel Support Vector Machines

The value returned by the KSVM is then mapped to the interval $[0, 1]$ to denote the probability of voxel v to belong to the organ

$$L(\vec{v}) = s\left(f\left(\vec{T}(\vec{v})\right)\right) = s\left(\sum_{i=1}^{m} \alpha_i l_i K\left(\vec{T}_i, \vec{T}(\vec{v})\right) + b\right)$$

Where $s(.)$ is a sigmoid function.

Kernel Support Vector Machines

The value returned by the KSVM is then mapped to the interval $[0, 1]$ to denote the probability of voxel v to belong to the organ

$$L(\vec{v}) = s\left(f\left(\vec{T}(\vec{v})\right)\right) = s\left(\sum_{i=1}^{m} \alpha_i l_i K\left(\vec{T}_i, \vec{T}(\vec{v})\right) + b\right)$$

Where $s(.)$ is a sigmoid function.

Kernel Support Vector Machines

The value returned by the KSVM is then mapped to the interval $[0, 1]$ to denote the probability of voxel v to belong to the organ

$$L(\vec{v}) = s\left(f\left(\vec{T}(\vec{v})\right)\right) = s\left(\sum_{i=1}^{m} \alpha_i l_i K\left(\vec{T}_i, \vec{T}(\vec{v})\right) + b\right)$$

Where $s(.)$ is a sigmoid function.

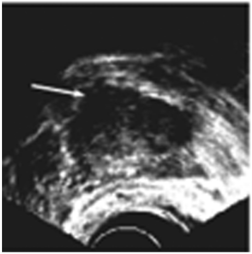

(a)

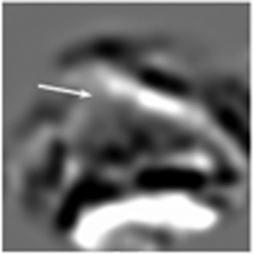

(b1)

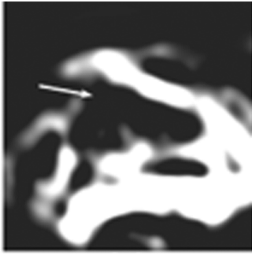

(b2)

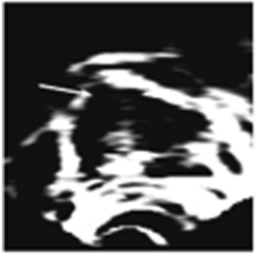

(b3)

(c)

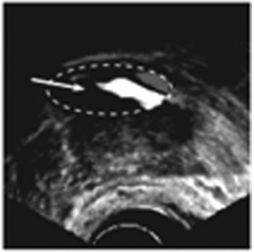

(d)

Since texture varies greatly along prostate boundaries

Instead of using a single G-SVM, one G-SVM is associated to each subsurface S_k in the deformable model

Number of subsurfaces should be limited (essentially because of time) for use in clinical applications

Since texture varies greatly along prostate boundaries

Instead of using a single G-SVM, one G-SVM is associated to each subsurface S_k in the deformable model

Number of subsurfaces should be limited (essentially because of time) for use in clinical applications

Since texture varies greatly along prostate boundaries

Instead of using a single G-SVM, one G-SVM is associated to each subsurface S_k in the deformable model

Number of subsurfaces should be limited (essentially because of time) for use in clinical applications

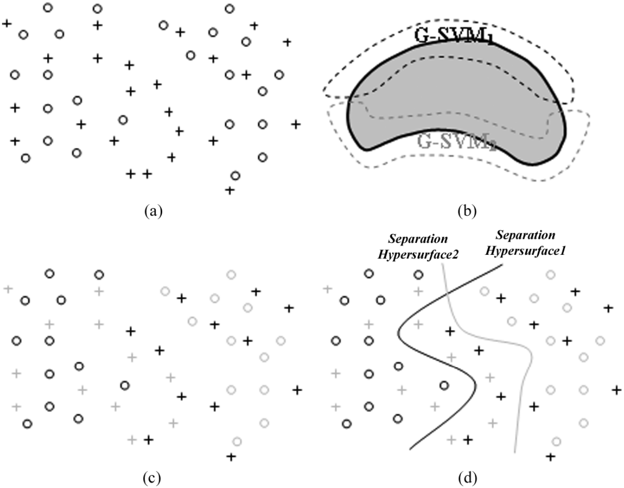
G-SVM$_1$
G-SVM$_2$
Separation Hypersurface2
Separation Hypersurface1
(a)
(b)
(c)
(d)

Once results of the G-SVM have been computed for the whole surface, an external energy term is computed

$$E^{ext}(\vec{P}_i) = w_{Sum}E_{Sum}(\vec{P}_i) + w_{Dist}E_{Dist}(\vec{P}_i)$$

$$\mathrm{E}_{Sum}(\vec{P}_i) = \left(\left(\frac{\sum_{\forall \vec{v} \in N(\vec{P}_i)} L(\vec{v};j))}{\sum_{\forall \vec{v} \in N(\vec{P}_i)} 1}\right) - 0.5\right)^2$$

$$E_{Dist}(\vec{P}_i) = \frac{\left(d(\vec{C}_P, \vec{P}_i) - d(\vec{C}_{NP}, \vec{P}_i)\right)^2}{R^2}$$

Once results of the G-SVM have been computed for the whole surface, an external energy term is computed

$$E^{ext}(\vec{P}_i) = w_{Sum} E_{Sum}(\vec{P}_i) + w_{Dist} E_{Dist}(\vec{P}_i)$$

$$\mathsf{E}_{Sum}(\vec{P}_i) = \left(\left(\frac{\sum_{\forall \vec{v} \in N(\vec{P}_i)} L(\vec{v};j))}{\sum_{\forall \vec{v} \in N(\vec{P}_i)} 1} \right) - 0.5 \right)^2$$

$$E_{Dist}(\vec{P}_i) = \frac{\left(d(\vec{C}_P, \vec{P}_i) - d(\vec{C}_{NP}, \vec{P}_i) \right)^2}{R^2}$$

Once results of the G-SVM have been computed for the whole surface, an external energy term is computed

$$E^{ext}(\vec{P}_i) = w_{Sum}E_{Sum}(\vec{P}_i) + w_{Dist}E_{Dist}(\vec{P}_i)$$

$$\mathsf{E}_{Sum}(\vec{P}_i) = \left(\left(\frac{\sum_{\forall \vec{v} \in N(\vec{P}_i)} L(\vec{v};j))}{\sum_{\forall \vec{v} \in N(\vec{P}_i)} 1}\right) - 0.5\right)^2$$

$$E_{Dist}(\vec{P}_i) = \frac{\left(d(\vec{C}_P, \vec{P}_i) - d(\vec{C}_{NP}, \vec{P}_i)\right)^2}{R^2}$$

E.S.B.C. Ang, V. Gluncic, A. Duque, M.E. Schafer & P. Rakic.
Prenatal exposure to ultrasound waves impacts neuronal migration in mice.
Proceedings of the National Academy of Sciences, vol. 103, no. 34, page 12903, 2006.

D. Fontanarosa, S. Van Der Meer, E. Harris & F. Verhaegen.
A CT based correction method for speed of sound aberration for ultrasound based image guided radiotherapy.
Medical Physics, vol. 38, page 2665, 2011.

C.R. Hill, J.C. Bamber & G. Haar.
Physical principles of medical ultrasonics.
Wiley, 2004.

Y. Zhan & D. Shen.
Deformable segmentation of 3-D ultrasound prostate images using statistical texture matching method.
Medical Imaging, IEEE Transactions on, vol. 25, no. 3, pages 256–272, 2006.